Acta Neuropathol (2017) 134:489–506
DOI 10.1007/s00401-017-1694-x

ORIGINAL PAPER

# IRE1 signaling exacerbates Alzheimer's disease pathogenesis

**Claudia Duran-Aniotz[1,2,3] · Victor Hugo Cornejo[1,2,3] · Sandra Espinoza[1,2,3] · Álvaro O. Ardiles[4] · Danilo B. Medinas[1,2,3] · Claudia Salazar[4] · Andrew Foley[1,3] · Ivana Gajardo[4] · Peter Thielen[5] · Takao Iwawaki[6] · Wiep Scheper[8,9] · Claudio Soto[7] · Adrian G. Palacios[4] · Jeroen J. M. Hoozemans[10] · Claudio Hetz[1,2,3,5,11]**

Received: 29 November 2016 / Revised: 7 March 2017 / Accepted: 7 March 2017 / Published online: 24 March 2017


**Abstract** Altered proteostasis is a salient feature of Alzheimer's disease (AD), highlighting the occurrence of endoplasmic reticulum (ER) stress and abnormal protein aggregation. ER stress triggers the activation of the unfolded protein response (UPR), a signaling pathway that enforces adaptive programs to sustain proteostasis or eliminate terminally damaged cells. IRE1 is an ER-located kinase and endoribonuclease that operates as a major stress transducer, mediating both adaptive and proapoptotic programs under ER stress. IRE1 signaling controls the expression of the transcription factor XBP1, in addition to degrade several RNAs. Importantly, a polymorphism in the XBP1 promoter was suggested as a risk factor to develop AD. Here, we demonstrate a positive correlation between the progression of AD histopathology and the activation of IRE1 in human brain tissue. To define the significance of the UPR to AD, we targeted IRE1 expression in a transgenic mouse model of AD. Despite initial expectations that IRE1 signaling may protect against AD, genetic ablation of the RNase domain of IRE1 in the nervous system significantly reduced amyloid deposition, the content of amyloid β oligomers, and astrocyte activation. IRE1 deficiency fully restored the learning and memory capacity of AD mice, associated with improved synaptic function and improved long-term potentiation (LTP). At the molecular level, IRE1 deletion reduced the expression of amyloid precursor protein (APP) in

C. Duran-Aniotz and V. H. Cornejo contributed equally to this work

**Electronic supplementary material** The online version of this article (doi:10.1007/s00401-017-1694-x) contains supplementary material, which is available to authorized users.

✉ Claudio Hetz
chetz@med.uchile.cl; chetz@hsph.harvard.edu
http://www.hetzlab.cl

1 Faculty of Medicine, Biomedical Neuroscience Institute, University of Chile, Santiago, Chile

2 Center for Geroscience, Brain Health and Metabolism, Santiago, Chile

3 Program of Cellular and Molecular Biology, Institute of Biomedical Sciences (Sector B, second floor), University of Chile, Independencia 1027, P.O.BOX 70086 Santiago, Chile

4 Centro Interdisciplinario de Neurociencia de Valparaiso, Universidad de Valparaiso, Valparaiso, Chile

5 Department of Immunology and Infectious diseases, Harvard School of Public Health, Boston, MA, USA

6 Division of Cell Medicine, Department of Life Science, Medical Research Institute, Kanazawa Medical University, 1-1 Daigaku, Uchinada, Kahoku, Ishikawa 920-0293, Japan

7 Department of Neurology, Mitchell Center for Alzheimer's disease and Related Brain Disorders, The University of Texas Houston Medical School at Houston, Houston, TX 77030, USA

8 Department of Clinical Genetics and Alzheimer Center, VU University Medical Center, Amsterdam, The Netherlands

9 Department of Functional Genomics, Center for Neurogenomics and Cognitive Research, VU University, Amsterdam, The Netherlands

10 Department of Pathology, VU University Medical Center, Amsterdam Neuroscience, Amsterdam, The Netherlands

11 Buck Institute for Research on Aging, Novato, CA 94945, USA

cortical and hippocampal areas of AD mice. In vitro experiments demonstrated that inhibition of IRE1 downstream signaling reduces APP steady-state levels, associated with its retention at the ER followed by proteasome-mediated degradation. Our findings uncovered an unanticipated role of IRE1 in the pathogenesis of AD, offering a novel target for disease intervention.

**Keywords** Alzheimer's disease · Amyloid β · Endoplasmic reticulum stress · Unfolded protein response · UPR · Proteostasis impairment

## Introduction

The clinical manifestation of Alzheimer's disease (AD) is triggered by the progressive loss of synaptic function followed by neuronal cell death. These events are mediated in part by the abnormal deposition of misfolded amyloid β (Aβ) peptide and hyperphosphorylated Tau in the brain of affected patients [4]. Although the etiology of AD remains poorly defined, accumulating evidence indicates that impairment in the buffering capacity of the proteostasis network is a salient feature of the disease that may drive abnormal protein aggregation [17, 20, 43]. Importantly, disruption of proteostasis is one of the hallmarks of aging, the main risk factor to develop AD [44, 54]. Alterations in protein clearance mechanisms, including autophagy and the lysosomal pathway, have been reported in AD models [50, 99, 100], which may contribute to the abnormal deposition of protein aggregates. The endoplasmic reticulum (ER) is the main subcellular compartment involved in protein folding and secretion, in addition to lipid synthesis and calcium storage. ER stress is emerging as a transversal pathological hallmark of AD, as reported in several studies of human postmortem brain tissue, in addition to most cellular and animal models of the disease (see below [13, 71]). In fact, disturbances to the function of the ER are proposed to contribute to neurodegeneration in other protein misfolding disorders (PMDs), including Parkinson, Huntington, amyotrophic lateral sclerosis (ALS), among other diseases [26, 34, 65].

To alleviate ER stress, cells activate an integrated signaling pathway known as the unfolded protein response (UPR), which aims to re-establish ER proteostasis by decreasing the load of misfolded proteins and preventing abnormal aggregation [96]. In doing so, the UPR controls many aspects of the secretory pathway including protein synthesis, processing, folding, quality control mechanisms, protein degradation pathways, trafficking, and lipid synthesis [32, 97]. Conversantly, under chronic or irreversible ER stress, the UPR triggers cell death by apoptosis [65, 89]. The most conserved UPR signaling branch is initiated by the ER stress transducer Inositol-requiring enzyme 1α (here referred to as IRE1). IRE1 is an ER-located kinase and endoribonuclease that under ER stress conditions autotransphosphorylates and homodimerizes, inducing a conformational change in the cytosolic region that activates its RNase domain. IRE1 signals through a unique mechanism involving the unconventional splicing of the mRNA encoding XBP1, deleting a 26-nucleotide intron [7, 51, 103]. This processing event shift the coding reading frame of the RNA leading to the expression of XBP1s, a potent transcription factor that transactivates a cluster of UPR-target genes [2, 48]. In addition, the RNase domain of IRE1 degrades multiple mRNAs and microRNAs, a process termed regulated IRE1-dependent decay (RIDD) [59]. IRE1 also mediates the crosstalk with other stress pathways as a scafold by binding to adapter proteins, highlighting the activation of the JNK and NF-*k*B pathways [65].

Several groups have reported that ER stress is a common pathological feature of AD (reviewed in [13, 71, 77]). For example, signs of UPR activation are observed in postmortem AD brain, depicting a direct correlation between the presence of hyperphosphorylated Tau and ER stress markers in cortical neurons [37, 63, 82, 87]. Moreover, studies in cell culture models of AD suggest that ER stress mediates in part the occurrence of neuronal loss triggered by Aβ, possibly due to altered calcium homeostasis [93], whereas accumulation of Tau may impair ER-associated degradation (ERAD) resulting in chronic ER stress [1]. Remarkably, human neurons derived from induced pluripotent stem cells of AD patients revealed that ER stress is a prominent feature of this disease model [46]. Importantly, the well-known effects of UPR signaling on protein translation repression were shown to contribute to the cognitive impairment observed in AD models involving activation of the stress sensor PERK and the phosphorylation of the protein translation initiation factor eIF2α [22, 26]. Other recent studies also indicated that targeting ER proteostasis provides protection in experimental models of AD [70].

A polymorphism in the *XBP1* promoter was identified as risk factor to develop AD in the Chinese population [45]. This polymorphism was previously associated with bipolar disorders and schizophrenia [21, 42, 45]. A significant increase in XBP1 mRNA splicing was reported in cortical areas from AD human brain [49], whereas another report suggested that XBP1 mRNA did not reach levels of healthy age-matched controls, showing reduced levels [75]. A transient upregulation of XBP1s levels was observed early in the disease process in the 5xFAD mouse model of AD. [75]. Although the functional contribution of IRE1 and XBP1 to AD pathology has not been well defined, a genomic screening to define the regulatory network governed by XBP1s identified a cluster of AD genes as possible direct targets, including amyloid precursor protein (APP), components of the α-secretase, cyclin-dependent kinase 5 (CDK5), in

addition to proteins involved in APP trafficking and maturation [2]. However, the possible implications of XBP1 to APP biology or Aβ production are unknown. Of note, the overexpression of XBP1s in flies protects against Aβ toxicity [8] and Tau overexpression in the eye [53], suggesting neuroprotective effects possibly mediated by an attenuation of ER stress levels. Although these studies suggest that IRE1 signaling may participate in AD, the direct involvement of this pathway to its pathogenesis remains to be established.

Here we have addressed the possible contribution of IRE1 to the development of AD using complementary approaches. Analysis of AD brain tissue revealed a linear correlation between the degree of neuropathology (Braak stages) and the phosphorylation of IRE1. Based on these results, we explored the functional consequences of targeting IRE1 activity in the context of AD. Conditional deletion of the RNase domain of IRE1 in the nervous system had dramatic effects in reducing amyloid load and the levels of Aβ soluble and insoluble species in a mouse model of AD. Moreover, signs of astrogliosis were also attenuated in AD animals when IRE1 was targeted. Importantly, these protective effects translated into an improvement of synaptic function and reduced memory deficits. At the mechanistic level, we demonstrated that IRE1/XBP1 signaling determines the steady-state levels of APP by regulating its degradation at the ER. Overall, our results uncovered a previously unanticipated role of IRE1 in AD and suggest that strategies to inhibit its activity may slow the progression of the disease.

## Materials and methods

### AD human tissue

Brain samples were obtained from The Netherlands Brain Bank in the Netherlands Institute for Neuroscience (Amsterdam, The Netherlands). Clinical diagnosis was defined according to DSM-III-R criteria and the severity of dementia was evaluated according to the Global Deterioration Scale of Reisberg. Neuropathological diagnosis was established using immunohistochemical staining, in addition to haematoxylin and eosin, Bodian, and/or Gallyas silver staining [86]. Pathology was evaluated according to a modified assessment of Braak and Alafuzoff and the Aβ staging of Thal [3, 5, 83]. For this study, non-demented control and AD cases were selected with Braak stages ranging from 0 to VI. Formalin-fixed paraffin-embedded tissue from the mid-hippocampus of 7 patients per Braak stage was selected. Sections (5-μm thick) were stained accordingly to [37]. Briefly, brain slices were incubated with primary antibody (IRE1 alpha [p Ser724], Novus Biologicals, Littleton CO, USA, 1:15000) and then incubated with secondary EnVision™ HRP goat anti-rabbit/mouse antibody (EV-GαM$^{HRP}$, DAKO). Digital images of the CA1 and subiculum region were obtained using an Olympus light microscope equipped with a Leica MC170HD digital camera. All neurons (positive and negative for p-IRE1) were counted in based on the presence of a nucleolus. Only neurons with a visible nucleolus were counted. The quantification analysis was determined by counting positive versus negative cell immunostaining for p-IRE1. Double immunolabeling was performed as described previously [63], and brain slices from CA1 region of AD were labeled with p-IRE1 and p-Tau (AT8 Ser202, Thr205, Thermo Fisher Scientific 1:100). Total neurons (AT8−/p-IRE1−), p-IRE1 single positive (AT8−/p-IRE1+), AT8 single positive (AT8+/p-IRE1−) and AT8/IRE1 (AT8+/p-IRE1+) double positive were counted in 9 AD cases (Braak V and VI). To perform real-time qPCR, total RNA was isolated from frozen tissue using TriPure isolation reagent (Roche Applied Science, Basel, Switzerland) following the manufacturer's specifications. Oligo(dT) primed cDNA was obtained using the SensiFAST™ cDNA Synthesis Kit (Bioline Reagents Ltd, London, UK) and 1 μg of total RNA input.

### Generation of transgenic mouse model of AD knockout for IRE1 RNase domain

IRE1 conditional knockout mice (the *Ern1* floxed animal) were described before [40]. These animals were crossed with Nestin-Cre transgenic mice to drive deletion of the *Ern1* in the nervous system. Then, IRE1$^{cKO}$ mice were crossed with the AD model 5xFAD animals (formerly JAX Stock No. 008730). All animals were generated on a pure C67/b5 background. 5xFAD mice overexpress two transgenes, which three mutations in human APP gene (Swedish, Florida and London Familial Alzheimer's Disease), and two in human Presenilin- 1 (PSEN1) gene (M146L + L286 V). These animals begin the accumulation of Aβ aggregates at 2 months of age. Increased amounts of senile plaques, synaptic degeneration, and neuroinflammation, in addition to the occurrence of cognitive impairment, are observed between 4 and 5 months of age [66]. Animals were housed in groups of maximum five in individually ventilated cages under standard conditions (22 °C, 12 h light–dark cycle) receiving food and water ad libitum. All animal manipulations were carried out in accordance to standard regulations and approved by the Animal Welfare Committee of the Faculty of Medicine of the University of Chile, Chile. Mice were sacrificed by $CO_2$ inhalation and all efforts were made to minimize suffering. Half-brain (left hemisphere) was frozen at −80 °C for biochemical

analyses, whereas the other half (right hemisphere) was stored for histological studies.

### Behavioral studies

Cognitive impairment was measured by the Morris Water Maze behavioral test as previously described [95]. In this assessment, animals learn to swim to a hidden platform under the water. Mice between 6 and 8 months of age were placed in the pool and allowed to explore it for 1 min. The testing room was equipped with spatial cues for orientation. This training procedure was performed 6 times a day for four consecutive days per animal. On day five, the platform was removed from the pool to measure the time that the animals spend in the target quadrant until the platform was found by the animal. Additionally, during the training phase, the time spent in finding the platform was also measured for each animal. Learning performance was measured as total latency, and the memory performance at the third and fourth day of training was also determined.

### Electrophysiology analysis

Hippocampal slices were prepared as we previously reported [58]. Six- to nine-month-old mice were deeply anesthetized with isoflurane, and their brains were quickly removed. Slices (350 μm) were dissected in ice-cold dissection buffer using a vibratome (Vibratome 1000 plus, Ted Pella Inc., CA, USA). Synaptic responses were evoked by stimulating the Schaffer collaterals with 0.2 ms pulses delivered through concentric bipolar stimulating electrodes, and recorded extracellularly in the stratum radiatum of the CA1 subfield as we recently described [58]. Basal synaptic transmission was assayed by determining input–output relationships from field excitatory postsynaptic potentials generated by gradually increasing the stimulus intensity; the input was measured as the peak amplitude of the fiber volley (FV), and the output was the initial slope of field excitatory postsynaptic potentials. Long-term potentiation (LTP) was induced by four-theta burst stimulation (10 trains of four pulses at 100 Hz; 5 Hz interburst interval) delivered at 0.1 Hz. LTP magnitude was calculated as the average (normalized to baseline) of the responses recorded 50–60 min after conditioning stimulation.

### Histological analysis

Fixed brains were collected in serial coronal section on a freezing cryostat at 25-μm-thick serial slices (10 sections/stain/animal) from lambda 0 to lambda −4 mm. After formic acid-induced epitope retrieval, primary antibody 4G8 was incubated over night at a 1:1000 dilution at room temperature (RT) (Biolegend, San Diego, CA, USA). HRP-linked secondary goat anti-mouse antibody at a 1:1000 dilution (Invitrogen, Carlsbad, CA, USA) was incubated for 2 h at RT. Peroxidase reaction was visualized using DAB Kit (Vector) following the manufacturer's instructions. Finally, sections were dehydrated in ascendant ethanol, cleared in xylene, and coverslipped with DPX mounting medium (Innogenex, San Ramon, CA, USA). For fibrillar Aβ quantification, sections were incubated in Thioflavin-S (ThS) solution (0.025 in 50% ethanol) for 10 min after defrost. Sections were dehydrated in ascendant ethanol, cleared in xylene, and coverslipped with DPX mounting medium (Innogenex, San Ramon, CA, USA). All samples were analyzed using an inverted epifluorescent microscope (Olympus IX71), and quantification was performed using the ImageJ software. Astrogliosis was visualized after staining with rabbit Monoclonal Anti-Glial Fibrillary Acidic Protein (GFAP) antibody at a 1:1000 dilution (Abcam, Cambridge, MA, USA). To quantify neuronal counts, samples were incubated with Cresyl Violet Acetate aqueous solution (Sigma) 0.1% for 10 min. Then, samples were washed with distilled water and EtOH 95% for 1 min. Dehydration was performed in EtOH 100% and cleared in xylene.

### ELISA quantification of amyloid-β species

Dissected brain was separated in cortical and hippocampal areas to generate the brain homogenates (BH). To measure $A\beta_{42}$ levels, the BH were processed using a previously described serial extraction protocol [23, 24]. 10% BH (cortex and hippocampus) were centrifuged in L100 K ultracentrifuge tubes (Beckman-Coulter, Brea, CA, USA) at 32,600 r.p.m for 1 h at 4 °C in a 42.2 Ti rotor. Supernatants were collected and pellets were resuspended in 70% formic Acid (Fisher Scientific, Waltham, MA, USA). Then, samples were centrifuged for 30 min and supernatants were collected. Formic acid fractions were diluted on 1 M Tris Buffer pH 11 (Sigma-Aldrich, St. Louis, MO) 20-fold to neutralize the samples. ELISA was used to determine the levels of $A\beta_{42}$ in brain (kit KHB3442, Invitrogen, Carlsbad, CA, USA) following the manufacturer's instructions. Finally, samples were measured using an ELISA reader (EL800 BIO-TEK, BioTek, Winooski, VT, USA) at 450 nm.

### Biochemical analysis of APP in brain homogenates

For filter-trap and Western blot analysis, BH were diluted in TEN (10 mM Tris–HCl, 1 mM EDTA, 100 mM NaCl, pH 8.0, supplemented with protease and phosphatase inhibitors) buffer containing 0.5% Nonidet P-40 and 50 mM iodoacetamide, sonicated, and quantified. Then, samples were treated or not with the thiol-reducing agent dithiothreitol (DTT) followed by filter-trap and Western blot analysis. For detergent solubility, the BH was diluted

in TEN buffer containing 0.5% Nonidet P-40 and submitted to centrifugation at 1000*g*, for 10 min followed by centrifugation of the supernatant at 16,900*g* for 45 min. Insoluble pellet was resuspended in TEN buffer containing 0.5% Nonidet P-40 and sonicated to wash off contaminants followed by another cycle of centrifugation. The pellet was then solubilized in TEN buffer containing 2% SDS and analyzed by Western blot. Membranes were blotted for APP and Aβ using 6E10 antibody (Biolegend, San Diego, CA, USA). HSP90 or β-actin were monitored as loading control (Santa Cruz Biotechnology, Santa Cruz, CA, USA).

### Cell culture experiments

We generated stable Neuro2a cell lines with reduced levels of XBP1 using shRNAs and the lentiviral expression vector pLKO.1 for puromycin selection (constructs described in [35, 94]). Tunicamycin (Tm) and cycloheximide (CHX) were purchased from Calbiochem EMB Bioscience Inc. MG132 was purchased from Sigma-Aldrich. We developed assays using the transient expression of human wild-type APP as EGFP fusion protein [6]. We transfected cells with Effectene (Qiagen) according to manufacturer's protocol, using between 0.8 and 1.0 μg of plasmid per well on a 6-well plate format. APP-GFP expression was analyzed in total cell extracts prepared in RIPA buffer (25 mM Tris pH 8.0, 150 mM NaCl, 0.1% SDS, 1% DOC and 1%NP-40) containing a protease inhibitor cocktail (Roche) with sonication, and then submitted to Western blot. The following antibodies and dilutions were used: anti-GFP, 1:3000 (Santa Cruz), anti-Ubiquitin 1:10000 (Santa Cruz), anti-XBP1 1:1000 (Covance, Princeton, NJ, USA), and anti-β-actin, 1:40000 (MP BioMedicals, Santa Ana, CA, USA).

### Statistical analyses

Data are expressed as mean ± SEM. After confirming normal distribution with Skewness/Kurtosis statistic test, Student's *t* test was used to analyze differences in histological and biochemical analyses of Aβ and APP. For behavioral studies, astrogliosis and cresyl quantification one-way ANOVA followed by Tukey's multiple comparison or Newman–Keuls multiple comparison post-test was used to measure significant differences. Two-way ANOVA followed by Bonferroni post-test was used in electrophysiological and behavioral experiments. Statistical analyses were performed using GraphPad Prism 5.0 software. Statistical differences were considered significant for values of $p < 0.05$.

## Results

### IRE1 phosphorylation correlates with Alzheimer's disease histopathology

Although the occurrence of ER stress has been reported in the brain of patients with advanced AD, the possible association between IRE1 activation and the progression of the disease has not been established. Importantly, previous studies indicated that expression XBP1 levels are associated with poor prognosis in several human cancers [10, 27, 72, 101], suggesting a diagnosis value. To assess the possible correlation between UPR activation and the degree of AD pathology, we evaluated IRE1 phosphorylation (a measure of its activation status) in human postmortem brain tissue using immunohistochemistry. Human brain slices from different AD stages (0–VI Braak stages) were evaluated in CA1 and subiculum areas (Fig. 1). Age, sex, clinical diagnosis, and Braak scores of AD cases and non-demented control subjects used in this study are listed in Table 1. Low or undetectable levels of IRE1 phosphorylation were found in the brain of healthy control subjects (Braak 0) (Fig. 1a). Remarkably, we observed a direct association between IRE1 phosphorylation levels and the Braak stage in AD human brain (Fig. 1b). Patients at Braak stage V and VI presented a strong activation of IRE1, where more than 40 and 55% of neurons were positive for phospho-IRE1 staining, respectively. These results suggest that the activation status of this stress transducer progresses with the evolution and severity of the disease. In addition, we monitored the levels of XBP1 mRNA splicing in AD brains. Consistent with our observations, *XBP1s* levels were increased in cortical areas of AD patients compared to control cases as measured by real-time PCR using total brain extracts (Supplementary Fig. S1). Moreover, we also confirmed that a fraction of neurons containing neurofibrillary tangles (stained with AT8 antibody) were positive for IRE1 phosphorylation (Fig. 1c). In addition, we performed detailed quantification on 9 AD cases (Braak 5 and 6) to determine the proportion of neurons that are single or double positive for AT8 and phosphorylated IRE1. We observed that 41% of all neurons are double positive, 7% are positive for phosphorylated IRE1, 24% are AT8 positive, whereas 28% were negative for the staining (Fig. 1c). Senile plaques were also stained using anti-Aβ clone IC16 [92], and as expected extracellular plaques did not colocalize with phosphorylated IRE1 signals (Supplementary Fig. 1b). Taken together, these results indicate that AD progression at the histopathological level is associated with chronic IRE1 activation in the brain.

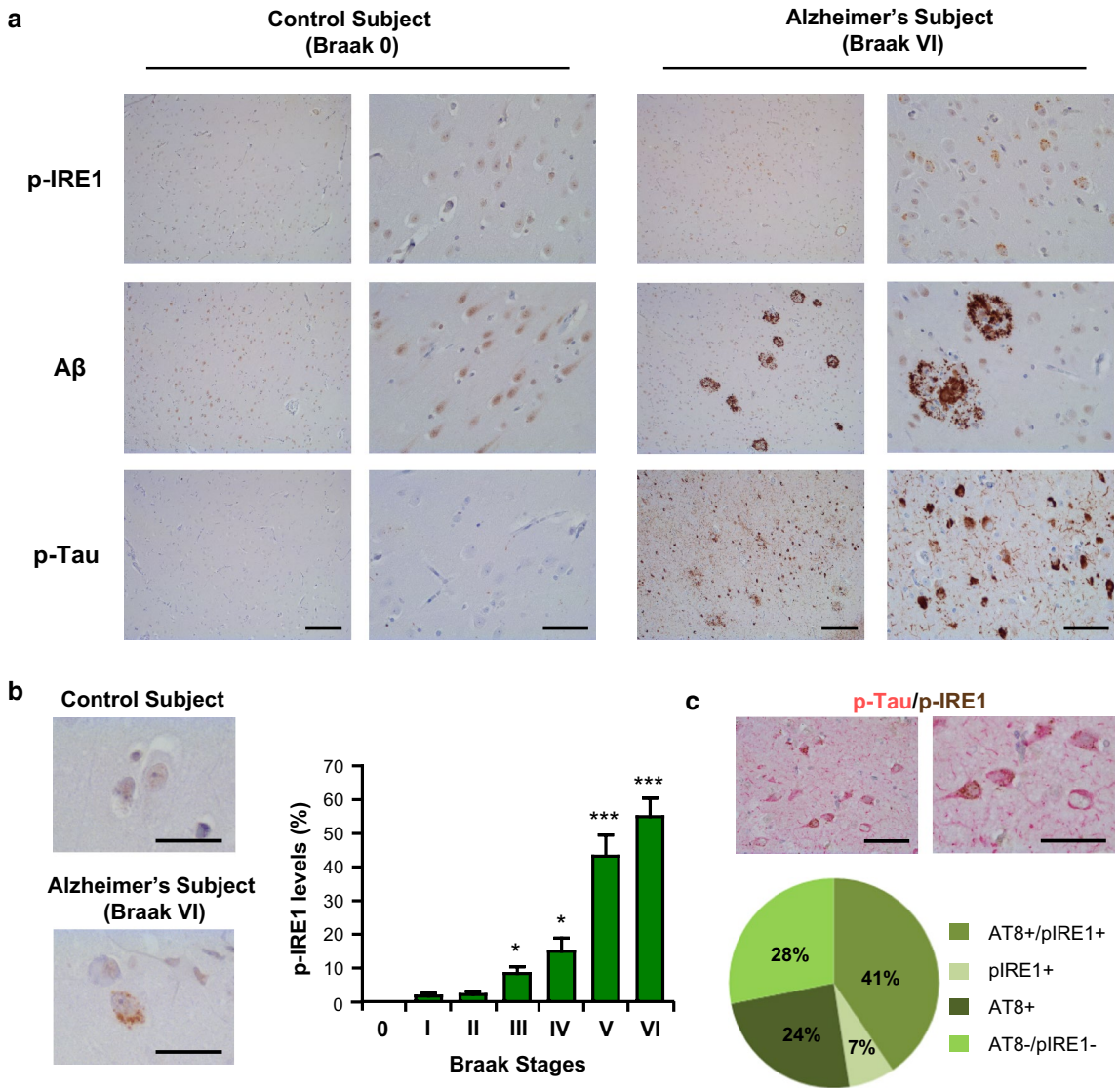


**Fig. 1** IRE1 phosphorylation correlates with Alzheimer's disease histopathological progression. **a** Phosphorylated IRE1 (p-IRE1), amyloid-β (Aβ), and phosphorylated Tau (p-Tau) levels were evaluated in the CA1 and subiculum region of the hippocampus of a control subject (Braak 0) and Alzheimer's subject (Braak VI). *Scale bar* 200 and 100 µm, respectively. **b** Human brain slices from patients at different AD stages (0–VI Braak stages) were stained for p-IRE and quantified ($n = 7$ per group) *Scale bar* 50 µm. **c** Double immunolabeling for p-Tau (*red*) with p-IRE1 (*brown*) in the CA1 region of AD cases (Braak VI, higher magnification right panel). *Scale bar* 100 µm (*left panel*) and 50 µm (*right panel*). Quantification of the percentage of neurons that were positive or not for AT8 and phosphorylated IRE1 is presented quantified in a total of 9 AD cases (Braak V and VI). A total of 85 neurons were counted on average per patient. Values in b are expressed as mean ± SEM and analyzed by Student's *t* test with comparison to Braak I ($n = 7$ per group). *$p < 0.05$; ***$p < 0.001$

## Targeting IRE1 in the nervous system reduces amyloid β load

To determine the significance of IRE1 signaling to AD, we generated a conditional knockout (cKO) mouse where the *Ern1* gene was deleted in neuronal progenitors using the Nestin-Cre system (here referred to as IRE1$^{cKO}$). This cKO model deletes exons 20–21 of *Ern1*, leading to the expression of a mutant protein that is devoid of its RNase domain [40]. IRE1$^{cKO}$ mice were born on a Mendelian rate and did not develop any obvious abnormalities (Table 2). Then, IRE1$^{cKO}$ animals were crossed with 5xFAD mice, which express a combination of five mutations on human APP and PSEN1 [66]. This transgenic mouse was chosen because it represents one of the few models that recapitulate most AD features including progressive Aβ deposition, cognitive impairment, synaptic dysfunction, brain inflammation, and neuronal loss during aging [66]. Offsprings from these breadings were viable and born on a Mendelian rate (Table 2). We confirmed the normal expression of the AD

**Table 1** Alzheimer's disease cases

| Case | Braak score for NFT | Braak score for amyloid | Clinical diagnosis | Age | Sex |
|---|---|---|---|---|---|
| 1 | 0 | | AD | 61 | M |
| 2 | 0 | B | AD | 86 | M |
| 3 | 0 | 0 | CON | 74 | M |
| 4 | 0 | 0 | CON | 49 | M |
| 5 | 0 | 0 | CON | 55 | M |
| 6 | 0 | 0 | CON | 76 | M |
| 7 | 0 | 0 | CON | 64 | F |
| 8 | I | B | CON | 87 | F |
| 9 | I | 0 | CON | 75 | F |
| 10 | I | A | N.A. | 66 | M |
| 11 | I | 0 | N.A. | 93 | M |
| 12 | I | A | CON | 92 | M |
| 13 | I | A/B | CON | 80 | M |
| 14 | I | N.A. | CON | 90 | M |
| 15 | II | A | CON | 70 | F |
| 16 | II | A | CON | 95 | F |
| 17 | II | 0 | CON | 94 | M |
| 18 | II | B | CON | 83 | F |
| 19 | II | B | CON | 84 | F |
| 20 | II | A | CON | 79 | M |
| 21 | II | C | CON | 80 | M |
| 22 | III | B | AD | 83 | M |
| 23 | III | A | CON | 81 | F |
| 24 | III | A | AD | 87 | F |
| 25 | III | B | CON | 95 | F |
| 26 | III | A | CON | 85 | F |
| 27 | III | A | CON | 90 | M |
| 28 | III | N.A. | CON | 81 | F |
| 29 | IV | B | AD | 96 | F |
| 30 | IV | N.A. | AD | 89 | M |
| 31 | IV | C | AD | 83 | F |
| 32 | IV | B | N.A. | 80 | F |
| 33 | IV | C | AD | 79 | M |
| 34 | IV | N.A. | CON | 88 | M |
| 35 | IV | N.A. | CON | 96 | M |
| 36 | V | C | AD | 85 | F |
| 37 | V | C | AD | 96 | F |
| 38 | V | C | AD | 95 | F |
| 39 | V | C | AD | 73 | M |
| 40 | V | C | AD | 80 | M |
| 41 | V | C | AD | 65 | F |
| 42 | V | C | AD | 79 | F |
| 43 | VI | N.A. | AD | 71 | M |
| 44 | VI | C | AD | 82 | F |
| 45 | VI | C | AD | 92 | F |
| 46 | VI | C | AD | 79 | M |
| 47 | VI | C | AD | 88 | M |
| 48 | VI | C | AD | 73 | F |
| 49 | VI | N.A. | AD | 79 | F |

Clinical data of cases investigated by histological analysis of post-mortem brain tissue (*NFT* neurofibrillary tangles, *CON* non-demented control, *AD* Alzheimer's disease, *N.A.* not available)

transgenes after deletion of the *Ern1* floxed alleles (Fig. 2a and Supplementary Fig. S2a). Additionally, we monitored the levels of XBP1 mRNA splicing in the brain of 5xFAD transgenic animals (Fig. 2b), observing a significant induction in 5xFAD that was IRE1-dependent.

To test the consequences of targeting IRE1 in the progression of AD pathogenesis, we evaluated Aβ load in the brain of IRE1$^{cKO}$/5xFAD animals. Immunohistochemical analysis of Aβ content using the 4G8 antibody indicated a 60% reduction in the cortex of IRE1$^{cKO}$/5xFAD mice compared to littermate control 5xFAD animals at 6 months of age (Fig. 2c). Quantification of the hippocampus also revealed a significant reduction of Aβ burden of approximately 50% upon targeting IRE1 (Fig. 2d). These results were confirmed by measuring the number of Aβ deposits per area in the cortex and hippocampus, revealing a strong reduction in the content of amyloid plaques (Fig. 2c, d, right panels). To assess the spatial distribution of amyloid plaques throughout the brain, we then quantified Aβ load in serial sections from the entire cortical and hippocampal areas (Fig. 2e, left and right panels, respectively). Remarkably, the effects of ablating IRE1 expression in the brain of AD mice were robust, reflected on a global decrease of Aβ burden.

We then evaluated the formation of fibrillar amyloid aggregates using thioflavin-S (ThS) staining. ThS-reactive deposits were observed mostly in cortex and hippocampus of 5xFAD transgenic animals at 6 months of age. ThS burden in IRE1$^{cKO}$/5xFAD followed the same pattern observed for 4G8 staining, showing a significant reduction of fibrillar aggregates in the cortex and hippocampus when compared with 5xFAD control mice (Fig. 3a, b). The distribution of ThS-positive plaques in these two brain areas was also monitored in serial sections (Supplementary Fig. S2b and S2c). To confirm the functional contribution of IRE1 to Aβ deposition, we generated an additional cohort of animals for analysis at 8 months of age. Again, we found a lower content of amyloid fibrillar deposits in IRE1$^{cKO}$/5xFAD mice compared to control animals in both cortical and hippocampal areas (Supplementary Fig. S2d and S2e, respectively).

Aβ-soluble oligomers are proposed as relevant neurotoxic species mediating synaptic dysfunction in AD [78]. To monitor the relative levels of soluble and insoluble Aβ, we performed serial extraction in detergents followed by $Aβ_{42}$ quantification in cortical and hippocampal homogenates using a specific human $Aβ_{42}$ ELISA assay. As predicted from our previous results, IRE1$^{cKO}$/5xFAD animals presented lower levels of oligomeric (PBS soluble) and fibrillar (formic acid insoluble) $Aβ_{42}$ species in both brain cortex (Fig. 3c) and hippocampus (Fig. 3d). Taken together, these results indicate that IRE1 deficiency significantly

**Table 2** Birth rate of the IRE1$^{cKO}$/5xFAD transgenic mice

| Genotype | Observed | Expected (%) | Observed (%) | Chi-square value |
|---|---|---|---|---|
| Wild-Type (WT) | 108 | 25 | 30.6 | 4.419 |
| IRE1$^{cKO}$ | 76 | 25 | 21.5 | 1.700 |
| 5xFAD | 102 | 25 | 28.9 | 2.142 |
| IRE1$^{cKO}$/5xFAD | 67 | 25 | 19 | 5.117 |

Genotypic distribution of offspring obtained from crosses of IRE1$^{flox/flox}$/5xFAD and IRE1$^{cKO}$ mice. Mendelian distribution was corroborated by Chi-square calculation

reduces the accumulation of Aβ in the brain of 5xFAD mice.

### Ablation of IRE1 in the brain ameliorates cognitive impairment in 5xFAD mice

In order to study the possible consequences of IRE1 deficiency on the behavioral impairment observed in 5xFAD model, we evaluated the learning and memory capacity of mice using the Morris Water Maze behavioral test. In line with the previous reports [67, 68], 5xFAD animals needed more time to find a hidden platform compared to non-transgenic littermate controls (Fig. 4a). Remarkably, IRE1$^{cKO}$/5xFAD mice showed a significant reversion of the memory impairment observed in this AD model with decreased total latency on the third and fourth days of training (Fig. 4b). The swimming velocity and exploration capacity of all experimental animals were similar to wild-type control mice (Supplementary Fig. S3), suggesting no motor or visual alterations of IRE1$^{cKO}$ mice.

One of the major targets of Aβ is dendritic spines, resulting in altered synaptic function [79]. To assess the consequences of ablating *Ern1* expression in the nervous system at the synaptic level, we performed electrophysiological measurements to monitor long-term potentiation (LTP) in the hippocampus. We recorded glutamatergic transmission evoked by Schaffer's collaterals stimulation to monitor field excitatory postsynaptic potentials (fEPSPs) in the CA1 region [29]. We confirmed that LTP, a long-lasting form of synaptic plasticity whose expression relies on postsynaptic mechanisms, was drastically impaired in 5xFAD mice after theta burst stimulation (Fig. 4c). Strikingly, deletion of the RNase domain of IRE1 in the nervous system restored LTP in 5xFAD mice (Fig. 4c). In addition, 5xFAD animals showed an abnormal basal synaptic transmission as indicated by a reduction in the input/output (I/O) function measured by comparing presynaptic fiber volley (FV) amplitudes and fEPSP slopes (postsynaptic activity) (Fig. 4d). Targeting IRE1 significantly reverted these electrophysiological alterations in 5xFAD mice (Fig. 4d). Thus, inhibition of IRE1 signaling prevented cognitive deficits observed in AD mice possibly by improving synaptic function and/or reducing Aβ levels.

### IRE1 deficiency reduces astrogliosis in AD mice

We then characterized other typical neuropathological alterations of AD in our experimental groups by monitoring astrocyte activation in the brain. Immunofluorescence analysis of GFAP staining indicated that astrogliosis was significantly induced in the hippocampus of 5xFAD mice (Fig. 5a). Deletion of IRE1 significantly attenuated astrocyte activation in the hippocampus almost to basal levels (Fig. 5b). In contrast, cortical areas presented a lower astrocytic reaction in this AD mouse model at 6 months of age, and did not show significant differences among the experimental groups (Fig. 5b). One of the advantages of using 5xFAD mice is the occurrence of morphological changes in neurons followed by late-onset neuronal loss [66]. We performed cresyl violet-staining to visualize global neuronal distribution in 5xFAD mice. According to previous studies [25, 66], we observed significant reduction in neuronal counts of Layer V of the brain cortex in 8-month-old 5xFAD mice (Fig. 5c). However, neuronal counts only slightly increased in the cortex of IRE1$^{cKO}$/5xFAD mice at this age (Fig. 5c), suggesting that the beneficial effects at the level of behavior and LTP are due to improved synaptic function rather than reduced toxicity of Aβ.

### IRE1 signaling controls APP expression levels

Overall, most of the phenotypes described here could be explained by a reduction in Aβ content, impacting therefore synaptic function and astrogliosis. Since we detected a general diminishment in the levels of both soluble and insoluble Aβ, our results may be explained by a modulation in APP expression levels or its processing. As described in Fig. 2a, the mRNA levels of the human APP and PSEN1 transgenes were not altered in IRE1$^{cKO}$ animals. To further explore the possible effects of IRE1 expression on AD features, we examined APP protein levels by Western blot analysis using the 6E10

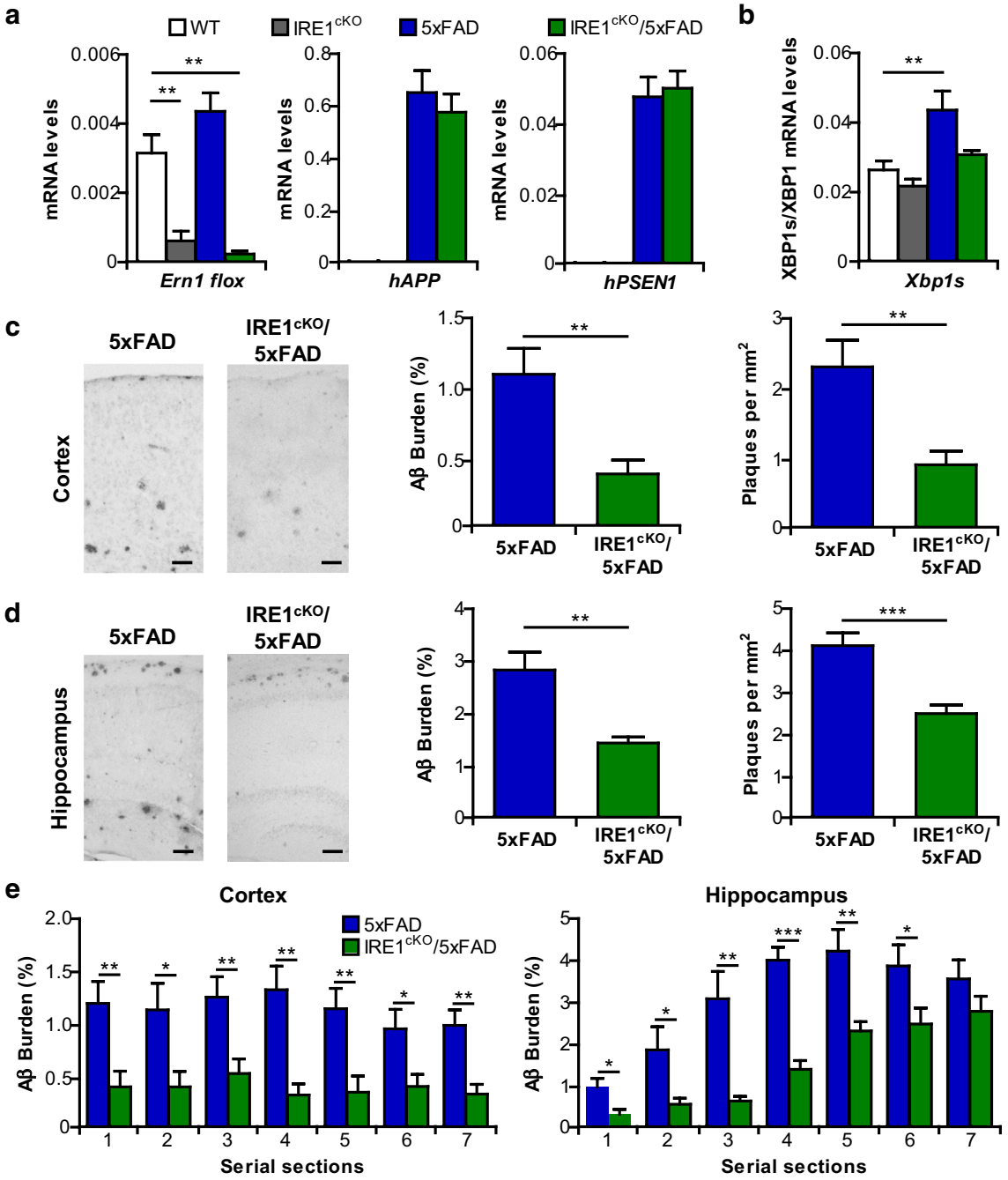


**Fig. 2** Targeting IRE1 in the nervous system reduces Aβ load in 5xFAD mice. IRE1 conditional knockout mice in the nervous system (IRE1$^{cKO}$) were crossed with 5xFAD mice to delete IRE RNase domain. **a** Transcriptional analysis was performed by real-time PCR in indicated animal groups to confirm the deletion of *Ern1* floxed allele and monitor the levels the human *APP* and *PSEN1* overexpression in brain cortex at 6–8 months of age. **b** The ratio between the mRNA levels of XBP1s and total XBP1 levels was quantified in experimental animals of 3 months of age ($n$ = 5–8 per group). Aβ deposits were quantified in cortical **c** and hippocampal **d** areas of 5xFAD and IRE1$^{cKO}$/5xFAD at 6 months of age. The burden of amyloid deposits and number of deposits was measured in serial brain slices (10 sections/staining/animal) using the 4G8 antibody against Aβ and expressed as mean value of the entire area (*middle and right panels*, respectively). *Scale bar* 100 μm. **e** Aβ distribution was determined in serial sections (1 to 7, rostral–caudal axis) from the entire cortex and hippocampus regions of animals presented in b and c. Values are expressed as mean ± SEM. 5xFAD ($n$ = 9) and IRE1$^{cKO}$/5xFAD ($n$ = 8). Data from **a** were analyzed by two-way ANOVA followed by Bonferroni post-test. Data from **c**, **d** and **e** were analyzed by Student's $t$ test. *$p < 0.05$; **$p < 0.01$; ***$p < 0.001$

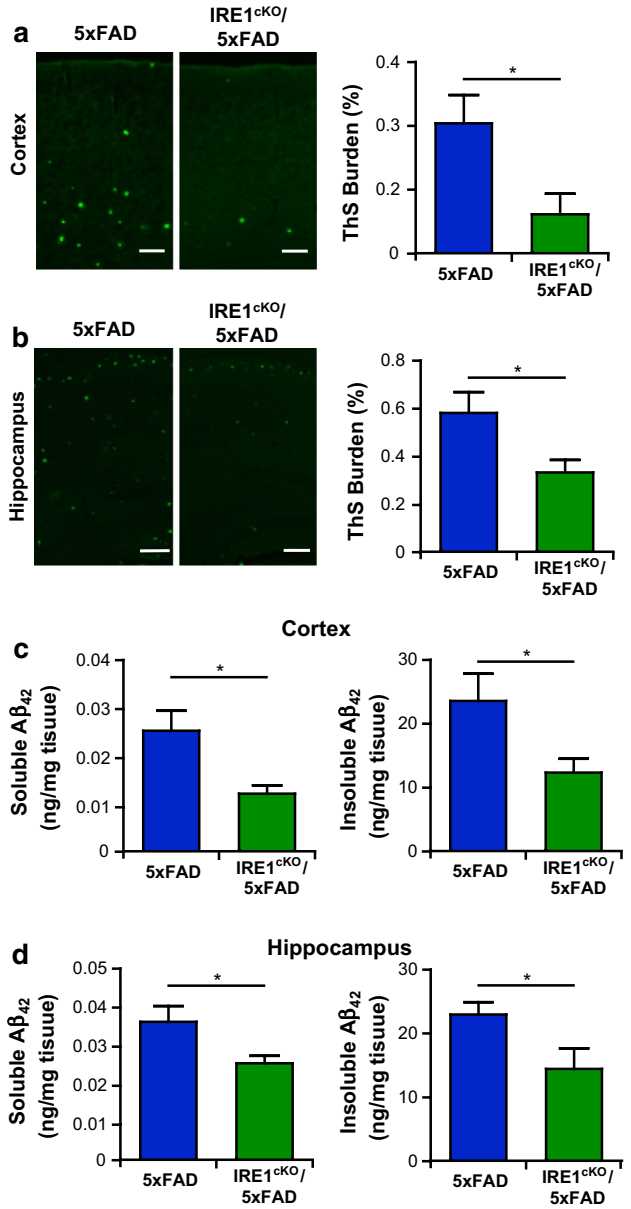


**Fig. 3** IRE1 deletion in the nervous system reduces fibrillar Aβ in 5xFAD mice. Amyloid deposits were quantified in cortical **a** and hippocampal **b** areas of 5xFAD and IRE1$^{cKO}$/5xFAD animals at 6 months of age. The burden of fibrillar Aβ was measured in serial brain slices (10 sections/staining/animal) using ThS staining and expressed as mean value for the area (right panels). *Scale bar* 100 μm. $Aβ_{42}$ levels were quantified in cortical **c** and hippocampal **d** homogenates after a serial extraction protocol (see methods) followed by detection using ELISA. Values are expressed as mean ± SEM. 5xFAD ($n$ = 6–15) and IRE1$^{cKO}$/5xFAD ($n$ = 6–9) animals. Data were analyzed by Student's $t$ test. *$p < 0.05$

antibody, which recognizes human APP and the Aβ peptide (Fig. 6a). Unexpectedly, an average reduction in the levels of APP of around 40–50% was observed in the cortex and hippocampus of IRE1$^{cKO}$/5xFAD animals compared to control AD mice (Fig. 6b, left and middle panel). Human APP in this biochemical analysis presented two bands, the lower band corresponding to the monomer, and a second high-molecular weight species possibly reflecting aggregated forms of the protein which was dramatically decreased upon IRE1 ablation (Fig. 6b, left and middle panel). In addition, we observed reduced levels of monomeric (~10 kDa) and dimeric Aβ species in the hippocampus of IRE1$^{cKO}$/5xFAD transgenic animals compared to control 5xFAD mice (Fig. 6b, right panel). To further characterize the properties of APP in our model, we carried out biochemical assays to detect protein aggregates. Filter-trap and centrifugal sedimentation analysis using brain cortex homogenates revealed aggregated forms of APP that are resistant to thiol reductants and non-ionic detergent (Supplementary Fig. S4a). Remarkably, this analysis confirmed that APP levels are significantly diminished in the brain of IRE1$^{cKO}$/5xFAD mice (Supplementary Fig. S4b). Since the mRNA levels of hAPP were not altered in IRE1$^{cKO}$/5xFAD animals, our results suggest that the UPR may control APP protein expression at the posttranscriptional level.

To gain mechanistic insights about the consequences of IRE1 signaling on APP levels, we performed in vitro studies using cell culture. To artificially enforce IRE1 downstream signaling outputs, we transiently transfected human APP fused with GFP (APP-GFP) together with an expression vector for the active spliced form of XBP1 (XBP1s) in the mouse neuroblastoma cell line Neuro2a. Overexpression of XBP1s increased steady-state levels of APP-GFP (Fig. 6c). As control, we monitored human *APP* mRNA levels using real-time PCR, observing equivalent expression in both pcDNA3 and XBP1s transfected cells (Fig. 6d). Similar results were obtained when 293T cells were co-transfected with APP-GFP and XBP1s expression vectors (Fig. 6e). As control, an inactive truncated form of XBP1s (XBP1mut) was employed (Fig. 6f).

We then performed loss-of-function experiments by knocking down XBP1 in Neuro2a cells through the stable delivery of a specific shRNA against XBP1 (shXBP1) [35] or control shRNA against luciferase (shLUC) using lentiviruses. Knockdown was confirmed by stimulating cells with the ER stress agent tunicamycin followed by Western blot analysis of XBP1s levels (Supplementary Fig. S5a). We transiently transfected APP-GFP in these shRNA cells and monitored its expression after 48 h. A dramatic reduction in APP-GFP levels was observed when XBP1 was knocked down as measured by Western blot (Fig. 6f) or FACS analysis to quantify the GFP signal (Fig. 6g). Importantly, the transfection efficiency in both shXBP1 and shLUC cells was similar (not shown). As control, we performed a rescue experiment by transfecting two concentrations of XBP1s plasmid, observing a partial recovery of APP-GFP levels

in shXBP1 cells (Fig. 6f). We also confirmed these results by expressing a human APP construct tagged with a FLAG sequence at the C-terminal region instead of GFP (Supplementary Fig. S5b). Thus, IRE1/XBP1 signaling increases APP protein expression.

### XBP1 regulates the degradation of APP

To determine the possible impact of IRE1 signaling on APP expression levels, we measured the half-life of APP in XBP1s overexpressing cells. We inhibited protein translation with cycloheximide (CHX) to follow the decay of APP-GFP (Fig. 7a). Consistent with the results presented in Fig. 6, a significant stabilization of APP-GFP was observed upon XBP1s overexpression (Fig. 7b). These results suggest that XBP1 may control APP degradation and/or maturation. Visualization of the subcellular distribution of APP-GFP revealed a vesicular pattern in control cells, whereas increased perinuclear localization was observed in shXBP1 cells (Fig. 7c). We used a sensitive method based on a confined displacement analysis algorithm to calculate colocalization coefficients of APP-GFP with the ER marker KDEL [73]. Quantification of Manders coefficient (M1) showed an average 0.30 index of colocalization between APP-GFP and KDEL under basal conditions, which was enhanced to 0.90 after knocking down XBP1 (Fig. 7c, right panel), suggesting retention of the protein at this early compartment of the secretory pathway.

We previously reported that knocking down XBP1 enhances macroautophagy levels, leading to the degradation of mutant proteins associated with ALS or Huntington's disease [35, 94]. In contrast with our previous results, blocking autophagy with a cocktail of lysosome inhibitors (pepstatin, E64D and bafilomycin $A_1$) did not recover the levels of APP in shXBP1 cells (Supplementary Fig. S5c). Similarly, inhibiting autophagy with 3-methyladenine did not increase APP levels in XBP1-deficient cells (Supplementary Fig. S5d). To control the efficiency of lysosomal inhibitors, we monitored the accumulation of p62, a classical substrate of the autophagy pathway. In addition, analysis of brain samples from $IRE1^{cKO}$/5xFAD mice did not reveal evident signs of autophagy induction (Supplementary Fig. S5e).

Abnormal protein products synthetized in the secretory pathway are often retained at the ER and then degraded by the proteasome through the ERAD machinery. Thus, we tested the consequences of inhibiting the proteasome with MG132 on APP levels in XBP1-deficient cells. As control for the inhibitors, protein ubiquitination was measured by Western blot in total cell lysates. Remarkably, a significant fold recovery of APP-GFP levels was observed upon proteasome inhibition in shXBP1 cells compared to control (Fig. 7d), suggesting that XBP1 deficiency may alter APP maturation at the ER leading to its degradation by the proteasome pathway. Taken together, these results suggest that the IRE1-XBP1 signaling branch enhances APP expression, which may contribute to accelerate AD pathogenesis.

## Discussion

AD is the most common type of senile dementia worldwide, however, no effective therapies are available for this devastating disease. The majority of diagnosed AD cases are categorized as sporadic, whereas 5% of all cases are considered familial [4]. The primary mechanisms responsible for the progressive neurodegeneration are starting to be understood, where alterations to the buffering capacity of the proteostasis network are emerging as a possible driver of AD pathogenesis. Importantly, aging is the main risk factor to develop the disease, and recent studies indicate that proteostasis alterations are one of the central pillars of aging [44, 54]. Multiple reports in model organisms indicate that the buffering capacity of the proteostasis network reduces during aging, resulting in chronic ER stress [20, 47]. Thus, proteostasis impairment may contribute to the abnormal accumulation of amyloid deposits and the formation of neurofibrillary tangles observed in AD [43]. Accumulating observations indicate that the occurrence of chronic ER stress correlates with AD pathology in human postmortem studies [77]. Although many studies in neurodegenerative conditions suggest a neuroprotective role of XBP1s, IRE1 signaling is emerging as a relevant controller of cell demise in various diseases including diabetes and retinal degeneration [28, 98].

Here, we have defined the role of IRE1, a major transducer of ER stress signals, to AD pathogenesis. We provide evidence indicating that IRE1 activation directly correlates with the severity of AD neuropathology. To functionally test the relevance of chronic IRE1 activation to AD pathogenesis, we performed extensive studies using genetic manipulation of the pathway in the 5xFAD mouse model. Targeting IRE1 signaling impacted all cardinal features of AD pathology, leading to (i) reduced amyloid deposits, (ii) improved cognitive and synaptic function, and (iii) attenuated astrogliosis. Together, our results suggest that chronic ER stress signaling may result in deleterious events by engaging prodegenerative UPR responses that exacerbate the progression of the disease. At the molecular level, we uncovered a novel output of the IRE1/XBP1 axis where it increases APP steady-state levels, possibly accelerating the amyloid cascade. These observations are in agreement with the previous findings indicating that XBP1s governs a transcriptional program that includes genes involved in

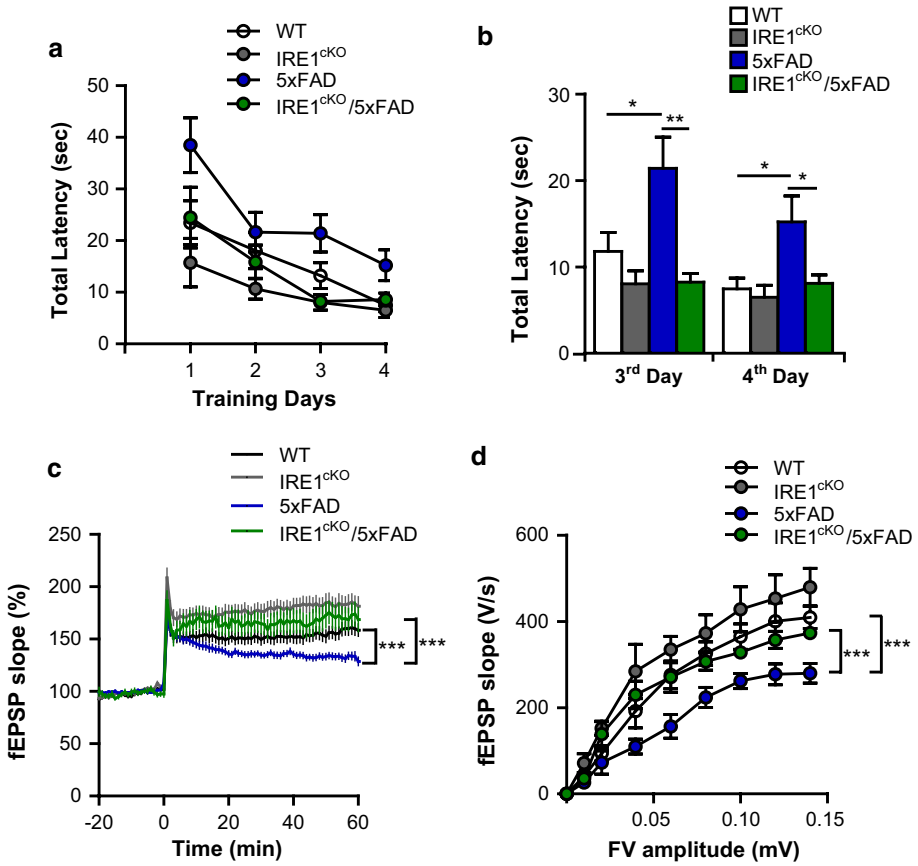


**Fig. 4** IRE1 ablation in the nervous system attenuates cognitive deficits and synaptic alterations of 5xFAD mice. **a** WT ($n = 15$), IRE1$^{cKO}$ ($n = 10$), 5xFAD ($n = 11$) IRE1$^{cKO}$/5xFAD ($n = 12$) animals were analyzed using the water maze behavioral test at 6 months of age. Learning performance was measured as total latency. **b** Memory performance at the third and fourth day of training. **c** Excitatory synaptic transmission was analyzed by long-term potentiation (LTP) in hippocampal slices from animals presented in a. Representative traces of the field excitatory postsynaptic potentials (fEPSPs) magnitude of hippocampal LTP induced by theta burst stimulation (TBS) protocol is shown ($n = 17$–$36$ slices from 4 to 6 animals per group). **d** Input–output relationship between fEPSP slope and fiber volley amplitude was monitored ($n = 20$–$40$ slices from 4 to 5 animals per group). Values are expressed as mean ± SEM. Data from b were analyzed by one-way ANOVA followed by Tukey's multiple comparison post-test. Data from c and d were analyzed by two-way ANOVA followed by Bonferroni post-test. *$p < 0.05$; **$p < 0.01$; ***$p < 0.001$

APP metabolism, trafficking, and processing [2]. We are currently interrogating the actual contribution of this cluster of XBP1s-target genes to APP expression. Importantly, the pathological consequences of chronic IRE1 signaling have been also mapped to sustained RIDD [28, 30, 52, 88]. Interestingly, one of canonical RIDD targets is Collagen 6 [36], a factor that protects against AD in mouse models [9, 11]. It remains to be determined if RIDD activity mediates part of the neuroprotective effects described here in 5xFAD mice.

Recent advances in the field have uncovered a novel activity of the proteostasis network and the UPR in modulating neuronal plasticity and synaptic function [16, 22, 26, 56]. The control of protein translation by eIF2α phosphorylation has been extensively implicated in memory consolidation, where ER stress-dependent (PERK) and -independent kinases (including PKR and GCN2) regulate LTP and memory consolidation (see examples in [15, 41, 84, 85]). Recent studies have shown that exacerbated phosphorylation of eIF2α through PERK signaling enhances cognitive decline in neurodegenerative conditions due to reduced synthesis of synaptic proteins as reported in prion disease models [61, 62]. In the context of AD, genetic inactivation of *Perk* in excitatory neurons of the forebrain and hippocampus improves cognitive function and synaptic plasticity of an AD model [56, 102]. Unexpectedly, the levels of Aβ deposition were not altered in that study. Besides, brain inflammation may engage PKR to exacerbate cognitive decline in AD possibly due to altered insulin signaling [55, 60]. In contrast, another report indicated that genetic ablation of GCN2 failed to rescue cognitive defects observed in 5xFAD mice, and actually enhanced the accumulation of amyloid plaques most likely due to PERK overactivation [18]. Other studies have linked the expression of PERK

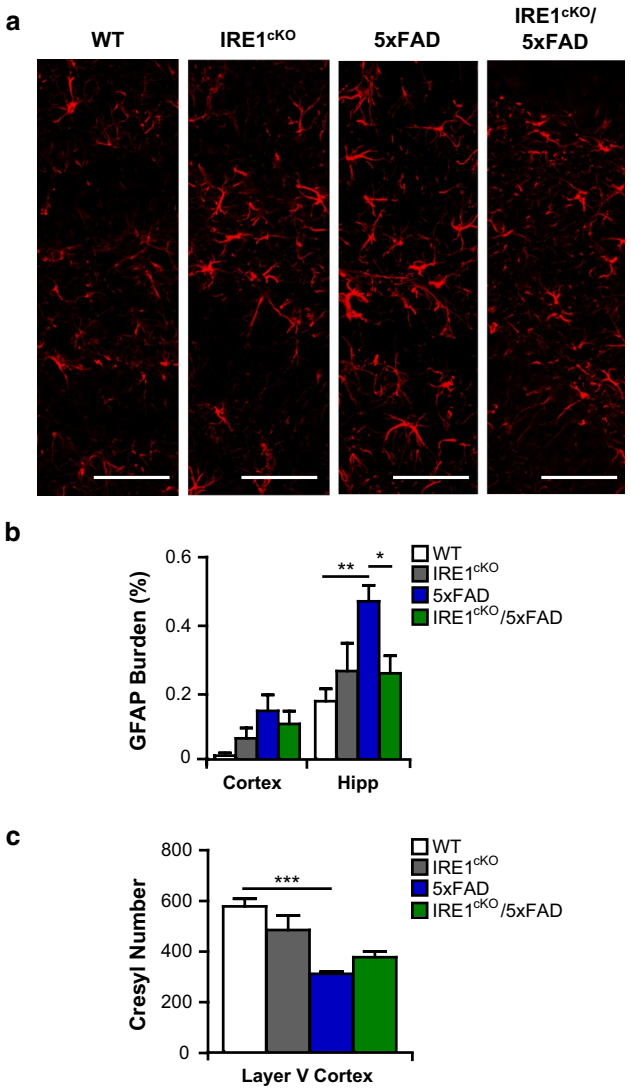


**Fig. 5** Effects of IRE1 ablation on astrogliosis in 5xFAD brain. **a** Astrocyte activation was analyzed in 5xFAD and IRE1$^{cKO}$/5xFAD animals and control mice at 6 months of age. **b** The astrocytic burden was measured using intensity of GFAP fluorescent staining ($n = 6$–11 per group). Scale bar: 200 µm in hippocampal areas. **c** Experimental animals were analyzed by cresyl staining to measure the number of cells in Layer V of the cortical region. ($n = 4$–6 per group). Values are expressed as mean ± SEM. Data were analyzed by one-way ANOVA followed by Newman–Keuls multiple comparison post-test. *$p < 0.05$; **$p < 0.01$. For correlation analysis in **b**, correlation test and the Pearson correlation coefficient were used to calculate R-value. *$p < 0.05$

with the upregulation of BACE1, bursting the accumulation of Aβ plaques and neuronal dysfunction in AD mice [19, 64]. In our hands, PERK signaling (assessed by eIF2α phosphorylation) was not engaged in 5xFAD, even in the context of IRE1 deficiency, suggesting the lack of compensatory events through PERK activation (Supplementary Fig. S6a and S6b). Similarly, active form of ATF6 was unchanged in our experimental animals (Supplementary Fig. S6c). Importantly, although chronic PERK signaling has been linked to neurodegenerative diseases such as Prion disease and AD [80], most studies have associated its signaling with neuroprotective effects in many disease conditions including ALS, multiple sclerosis, and mechanical injury to the nervous system (reviewed in [12, 34]). Taken together with our current study, a complex model can be inferred where different UPR signaling outputs initiated by PERK and IRE1 negatively impact synaptic function, APP metabolism, and amyloid deposition in AD possibly involving independent and distinct mechanisms of action.

Recently, our group identified a novel function of XBP1 in regulating learning and memory-related process in the hippocampus [58]. This novel activity of XBP1s in the brain was mapped to the transcriptional control of the neurotrophic factor BDNF. In contrast, as presented here, phenotypic characterization of IRE1$^{cKO}$ mice in the water maze and LTP assays did not depict any disruption at basal levels. In agreement with this, we did not observe any significant deregulation of BDNF in the hippocampus of IRE1$^{cKO}$ mice (Supplementary Fig. 6d). This puzzling observation is in agreement with previous finding indicating that the phenotypes of IRE1- and XBP1-deficient animals do not fully match (reviewed in [14]). For example, *Xbp1* deficiency is embryonic lethal [74] and its conditional deletion leads to severe alterations to pancreatic function, immunoglobulin secretion, salivary glands among other defects [14]. In sharp contrast, the lethality of *Ern1* null mice can be fully rescued by the selective expression of IRE1 in the placenta [40]. IRE1-deficient animals presented only minor alterations to specialized secretory cells [39], suggesting that XBP1 may have independent functions of IRE1. It has been also suggested that many of the phenotypes described in XBP1 deficient animals may be explained by the overactivation of IRE1, leading to sustained RIDD [14].

The involvement of the UPR in neurodegeneration is complex and may depend on the signaling pathway affected and the disease context [34, 77, 80]. Although XBP1 has been targeted in various neurodegenerative diseases, the impact of IRE1 as a therapeutic target has not been explored in any brain disease. For example, genetic ablation of *Xbp1* in the nervous system delays experimental ALS and Huntington's disease possibly due to compensatory changes that upregulate autophagy [35, 94]. In contrast, XBP1 expression enhances locomotor recovery after mechanical damage to the peripheral [69] and central nervous system [91]. Artificial overexpression of XBP1s also protects against Parkinson's disease [76, 90], glaucoma, and retinal degeneration [38, 81]. In the context of prion disease, XBP1 deficiency did not modify prion misfolding and propagation [33]. Overall,

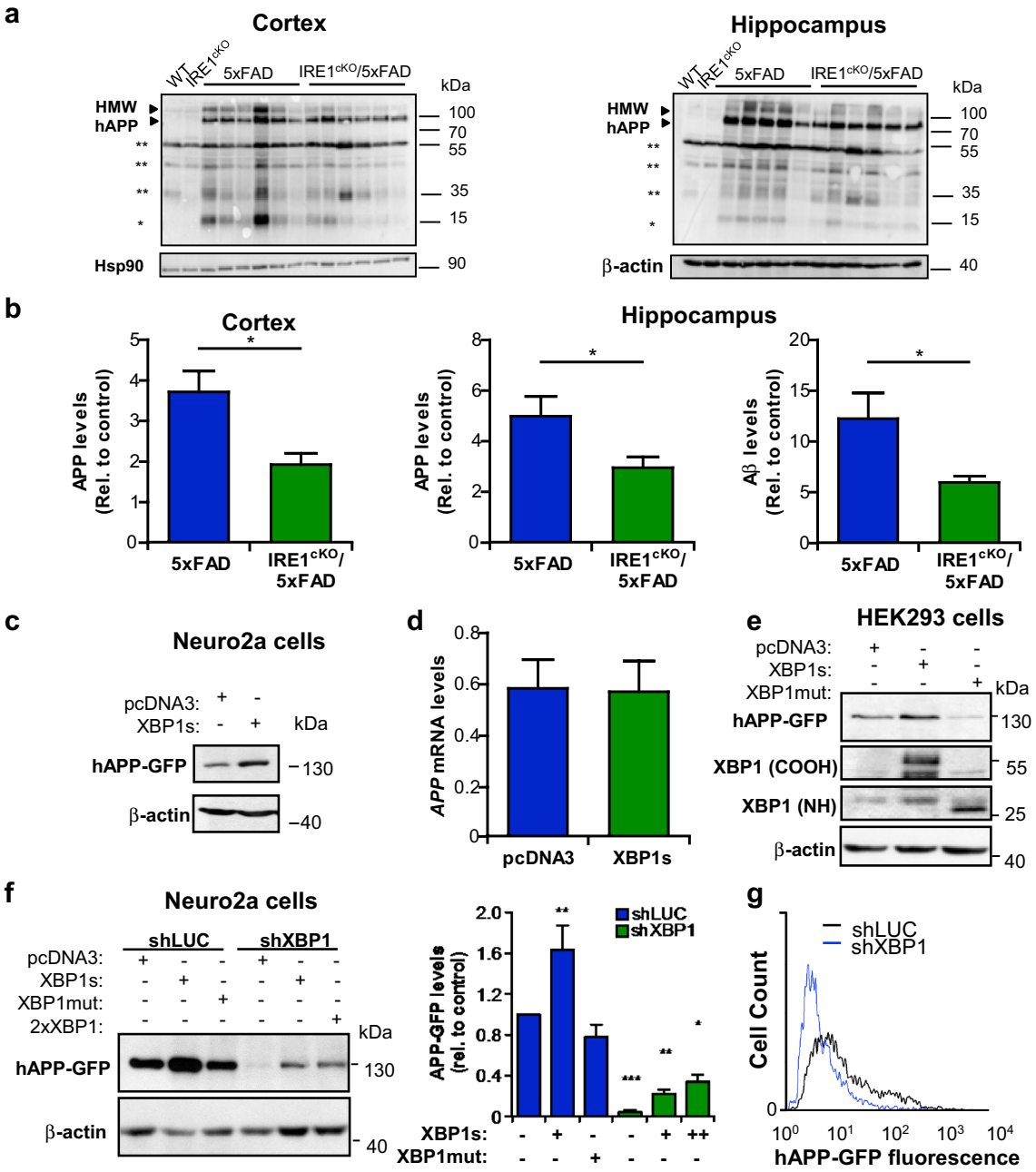


**Fig. 6** IRE1 signaling enhances APP expression. **a** APP total levels were monitored in the cortex and hippocampus of 5xFAD, IRE1$^{cKO}$/5xFAD and littermate control animals by Western blot using 6E10 antibody. Aβ species are indicated with *one asterisk*, whereas unspecific bands are indicated with *two asterisks*. **b** Quantification of HMW APP species is presented in *left* and *middle panels*. Relative levels of low-molecular-weight Aβ species were quantified in hippocampus of IRE1$^{cKO}$/5xFAD and 5xFAD mice by Western blot analysis of animals presented in Fig. 6a (*right panel*). **c** Neuro2a cells were co-transfected with an expression vector for APP fused with GFP (hAPP-GFP) and empty (pcDNA3) vector or XBP1s construct. APP levels were monitored by Western blot analysis after 48 h of transfection. **d** mRNA levels of human *APP* of cells presented in **c** were determined by real-time qPCR. **e** HEK293 cells were transiently co-transfected with APP-GFP expression vector and empty (pcDNA3) vector or construct for XBP1s or an inactive mutant form of the protein (XBP1mut). After 48 h of transfection, cells were lysed for Western blot analysis using anti-GFP and anti-XBP1, detecting both C- and N- terminal of the protein ($n = 3$). **f** shLUC and shXBP1 Neuro2a cells were transiently co-transfected with APP-GFP expression vector and empty (pcDNA3) vector or construct for XBP1s or XBP1mut as indicated. After 48 h of expression, cells were lysed for Western blot analysis using anti-GFP antibody. Histogram shows quantification of band intensity in each condition normalized to non-transfected shLUC cells ($n = 4$). **g** The levels of APP-GFP expression were monitored in shLUC and shXBP1 cells after 48 h of transfection using FACS analysis. Values are expressed as mean ± SEM. Data were analyzed by Student's *t* test using for statistical significance: $^*p < 0.05$ *HMW* High-molecular weight

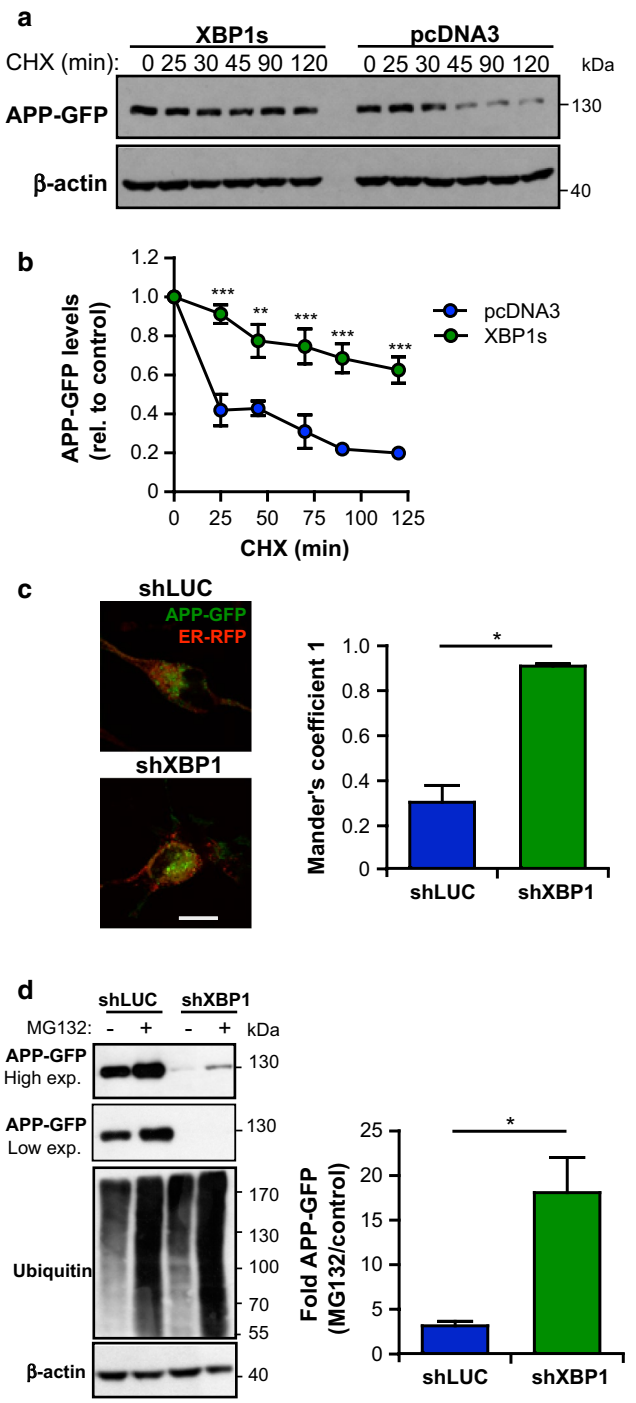


**Fig. 7** The IRE1/XBP1 pathway controls APP steady-state levels. **a**▶ Neuro2a cells were co-transfected with hAPP-GFP expression vector and empty pcDNA3 or XBP1 s construct and treated with cycloheximide (CHX, 50 µm/mL). At indicated time points, cells were lysed for Western blot analysis using anti-GFP antibody. **b** Quantification of APP expression was performed in experiments presented in a. β-Actin levels were monitored as loading control ($n = 4$). **c** Neuro2a shLUC and shXBP1 cell were transiently co-transfected with expression vectors for APP-GFP and ER-RFP, a construct that express RFP fused with KDEL retention signal. Cells were fixed and imaged using confocal microscopy. The *scale bar* represents 10 µm. Mander's 1 coefficient was calculated to determine the colocalization index (*right panel*). Cells with higher GFP signal were used for proper analysis comparison. **d** Neuro2a shLUC and shXBP1 cells were transiently transfected with APP-GFP expression vector. Cells were re-plated at 24 h post-transfection and then treated with MG132 (1 µM) for 16 h followed by Western blot analysis. Ubiquitin levels were monitored as positive control for proteasome inhibition. APP-GFP levels were quantified using β-actin levels as loading control and plotted as a fold change to untreated cells. Values are expressed as mean ± SEM. Data were analyzed by Student's *t* test using for statistical significance: $*p < 0.05$; $**p < 0.01$; $***p < 0.001$

our results support the idea that sustained activation of IRE1 may amplify the neuropathological process underlying AD, modulating in part APP degradation and/or its maturation. We reason that altered neuronal proteostasis during aging may operate as a molecular switch that triggers abnormal levels of ER stress and activates detrimental signaling events mediated by PERK and IRE1 that exacerbate the progression of AD. Our current study represents the first effort to uncover the potential therapeutic implication of inhibiting IRE1 signaling on a neurodegenerative condition. Since there are no treatments available that can reverse or block the progression of AD, new concepts need to be tested to identify druggable targets. Importantly, recent drug discovery efforts led to the identification of novel IRE1 RNase and kinase inhibitors that have been exploited for cancer treatment [31, 57]. Recently, the significance of IRE1 inhibition for disease treatment was expanded to diabetes and retinal degeneration using pharmacological approaches [28]. Although AD still lacks solid animal models to mimic all aspects of the disease, our conclusions are based on the analysis of human AD tissue, functional manipulation in mice followed by histological, biochemical, and behavioral analysis, in addition to mechanistic studies in cell culture models. In summary, here we provide compelling evidence indicating that targeting of a central ER stress transducer alleviates experimental AD and promises potential to design alternative strategies to ameliorate disease progression.

**Acknowledgements** We thank Javiera Ponce for technical support in animal care supervision. We also thank Dr. Alejandra Alvarez from The Pontifical Catholic University of Chile for the use of behavioral facilities and Dr. Patricia Burgos from University Austral of Chile for providing APP-GFP constructs. Additionally, we would like to thank Dr. Rodrigo Morales, Dr. Ines Moreno-Gonzalez, and Dr. Mohammad Shahnawaz of University of Texas Houston Medical School at Houston and Dr. Rene Vidal and Dr. Gabriela Martinez Bravo of University of Chile, for providing helpful support. We also thank the Netherlands Brain Bank for supplying the human brain tissue, Wouter Gerritsen, Tjado Morrema, Kimberley Ummenthum, and Fabian Bangel for technical assistance in human studies. This work was directly funded by FONDAP program 15150012, CONICYT-Brazil cooperation Grant 441921/2016-7, Office of Naval Research Global (ONR-G)

N62909-16-1-2003, Millennium Institute P09-015-F, FONDEF ID16I10223 (CH) and FONDECYT no 11160760 (CDA). We also thank the support Muscular Dystrophy Association 382453, FONDECYT No. 1140549, and ALSRP Therapeutic Idea Award AL150111, U.S. Air Force Office of Scientific Research FA9550-16-1-0384, European Commission R&D, MSCA-RISE #734749 (CH), FONDECYT Grant No. 3160725 (VHC), FONDECYT Grant No. 11150776 (AOA), and FONDECYT Grant No. 11150579 (DBM) and Rotary International Global Grant for Disease Treatment and Prevention (AF) and Millennium Institute ICM-P09-022-F (AP).

**Compliance with ethical standards**

**Conflict of interest** The authors declare that they have no conflicts of interest.

## References

1. Abisambra JF, Jinwal UK, Blair LJ et al (2013) Tau accumulation activates the unfolded protein response by impairing endoplasmic reticulum-associated degradation. J Neurosci 33:9498–9507. doi:10.1523/JNEUROSCI.5397-12.2013
2. Acosta-Alvear D, Zhou Y, Blais A et al (2007) XBP1 controls diverse cell type- and condition-specific transcriptional regulatory networks. Mol Cell 27:53–66. doi:10.1016/j.molcel.2007.06.011
3. Alafuzoff I, Pikkarainen M, Neumann M et al (2015) Neuropathological assessments of the pathology in frontotemporal lobar degeneration with TDP43-positive inclusions: an interlaboratory study by the BrainNet Europe consortium. J Neural Transm (Vienna) 122:957–972. doi:10.1007/s00702-014-1304-1
4. Ballard C, Gauthier S, Corbett A et al (2011) Alzheimer's disease. Lancet 377:1019–1031. doi:10.1016/S0140-6736(10)61349-9
5. Braak H, Braak E (1991) Neuropathological stageing of Alzheimer-related changes. Acta Neuropathol 82:239–259
6. Burgos PV, Mardones GA, Rojas AL et al (2010) Sorting of the Alzheimer's disease amyloid precursor protein mediated by the AP-4 complex. Dev Cell 18:425–436. doi:10.1016/j.devcel.2010.01.015
7. Calfon M, Zeng H, Urano F et al (2002) IRE1 couples endoplasmic reticulum load to secretory capacity by processing the XBP-1 mRNA. Nature 415:92–96. doi:10.1038/415092a
8. Casas-Tinto S, Zhang Y, Sanchez-Garcia J et al (2011) The ER stress factor XBP1 s prevents amyloid-beta neurotoxicity. Hum Mol Genet 20:2144–2160. doi:10.1093/hmg/ddr100
9. Cescon M, Chen P, Castagnaro S, Gregorio I, Bonaldo P (2016) Lack of collagen VI promotes neurodegeneration by impairing autophagy and inducing apoptosis during aging. Aging (Albany NY) 8:1083–1101. doi:10.18632/aging.100924
10. Chen X, Iliopoulos D, Zhang Q et al (2014) XBP1 promotes triple-negative breast cancer by controlling the HIF1alpha pathway. Nature 508:103–107. doi:10.1038/nature13119
11. Cheng JS, Dubal DB, Kim DH et al (2009) Collagen VI protects neurons against Abeta toxicity. Nat Neurosci 12:119–121. doi:10.1038/nn.2240
12. Clayton BL, Popko B (2016) Endoplasmic reticulum stress and the unfolded protein response in disorders of myelinating glia. Brain Res 1:594–602. doi:10.1016/j.brainres.2016.03.046
13. Cornejo VH, Hetz C (2013) The unfolded protein response in Alzheimer's disease. Semin Immunopathol 35:277–292. doi:10.1007/s00281-013-0373-9
14. Cornejo VH, Pihan P, Vidal RL, Hetz C (2013) Role of the unfolded protein response in organ physiology: lessons from mouse models. IUBMB Life 65:962–975. doi:10.1002/iub.1224
15. Costa-Mattioli M, Gobert D, Harding H et al (2005) Translational control of hippocampal synaptic plasticity and memory by the eIF2alpha kinase GCN2. Nature 436:1166–1173. doi:10.1038/nature03897
16. Costa-Mattioli M, Sossin WS, Klann E, Sonenberg N (2009) Translational control of long-lasting synaptic plasticity and memory. Neuron 61:10–26. doi:10.1016/j.neuron.2008.10.055
17. Cuanalo-Contreras K, Mukherjee A, Soto C (2013) Role of protein misfolding and proteostasis deficiency in protein misfolding diseases and aging. Int J Cell Biol 2013:638083. doi:10.1155/2013/638083
18. Devi L, Ohno M (2013) Deletion of the eIF2alpha Kinase GCN2 fails to rescue the memory decline associated with Alzheimer's disease. PLoS OnE 8:e77335. doi:10.1371/journal.pone.0077335
19. Devi L, Ohno M (2014) PERK mediates eIF2alpha phosphorylation responsible for BACE1 elevation, CREB dysfunction and neurodegeneration in a mouse model of Alzheimer's disease. Neurobiol Aging 35:2272–2281. doi:10.1016/j.neurobiolaging.2014.04.031
20. Douglas PM, Dillin A (2010) Protein homeostasis and aging in neurodegeneration. J Cell Biol 190:719–729. doi:10.1083/jcb.201005144
21. Du J, Duan S, Wang H et al (2008) Comprehensive analysis of polymorphisms throughout GAD1 gene: a family-based association study in schizophrenia. J Neural Transm 115:513–519. doi:10.1007/s00702-007-0844-z
22. Duran-Aniotz C, Martinez G, Hetz C (2014) Memory loss in Alzheimer's disease: are the alterations in the UPR network involved in the cognitive impairment? Front Aging Neurosci 6:8. doi:10.3389/fnagi.2014.00008
23. Duran-Aniotz C, Morales R, Moreno-Gonzalez I et al (2014) Aggregate-depleted brain fails to induce Abeta deposition in a mouse model of Alzheimer's disease. PLoS One 9:e89014. doi:10.1371/journal.pone.0089014
24. Duran-Aniotz C, Morales R, Moreno-Gonzalez I, Hu PP, Soto C (2013) Brains from non-Alzheimer's individuals containing amyloid deposits accelerate Abeta deposition in vivo. Acta Neuropathol Commun 1:76. doi:10.1186/2051-5960-1-76
25. Eimer WA, Vassar R (2013) Neuron loss in the 5XFAD mouse model of Alzheimer's disease correlates with intraneuronal Abeta42 accumulation and Caspase-3 activation. Mol Neurodegener 8:2. doi:10.1186/1750-1326-8-2
26. Freeman OJ, Mallucci GR (2016) The UPR and synaptic dysfunction in neurodegeneration. Brain Res 1:530–537. doi:10.1016/j.brainres.2016.03.029
27. Gambella M, Rocci A, Passera R et al (2014) High XBP1 expression is a marker of better outcome in multiple myeloma patients treated with bortezomib. Haematologica 99:e14–16. doi:10.3324/haematol.2013.090142
28. Ghosh R, Wang L, Wang ES et al (2014) Allosteric inhibition of the IRE1alpha RNase preserves cell viability and function during endoplasmic reticulum stress. Cell 158:534–548. doi:10.1016/j.cell.2014.07.002
29. Granger AJ, Nicoll RA (2014) Expression mechanisms underlying long-term potentiation: a postsynaptic view, 10 years on. Philos Trans R Soc Lond B Biol Sci 369:20130136. doi:10.1098/rstb.2013.0136
30. Han D, Lerner AG, Vande Walle L et al (2009) IRE1alpha kinase activation modes control alternate endoribonuclease outputs to determine divergent cell fates. Cell 138:562–575. doi:10.1016/j.cell.2009.07.017
31. Hetz C, Chevet E, Harding HP (2013) Targeting the unfolded protein response in disease. Nat Rev Drug Discov 12:703–719. doi:10.1038/nrd3976

32. Hetz C, Chevet E, Oakes SA (2015) Proteostasis control by the unfolded protein response. Nat Cell Biol 17:829–838. doi:10.1038/ncb3184
33. Hetz C, Lee AH, Gonzalez-Romero D et al (2008) Unfolded protein response transcription factor XBP-1 does not influence prion replication or pathogenesis. Proc Natl Acad Sci USA 105:757–762. doi:10.1073/pnas.0711094105
34. Hetz C, Mollereau B (2014) Disturbance of endoplasmic reticulum proteostasis in neurodegenerative diseases. Nat Rev Neurosci 15:233–249. doi:10.1038/nrn3689
35. Hetz C, Thielen P, Matus S et al (2009) XBP-1 deficiency in the nervous system protects against amyotrophic lateral sclerosis by increasing autophagy. Genes Dev 23:2294–2306. doi:10.1101/gad.1830709
36. Hollien J, Lin JH, Li H et al (2009) Regulated Ire1-dependent decay of messenger RNAs in mammalian cells. J Cell Biol 186:323–331. doi:10.1083/jcb.200903014
37. Hoozemans JJ, van Haastert ES, Nijholt DA et al (2009) The unfolded protein response is activated in pretangle neurons in Alzheimer's disease hippocampus. Am J Pathol 174:1241–1251. doi:10.2353/ajpath.2009.080814
38. Hu Y, Park KK, Yang L et al (2012) Differential effects of unfolded protein response pathways on axon injury-induced death of retinal ganglion cells. Neuron 73:445–452. doi:10.1016/j.neuron.2011.11.026
39. Iwawaki T, Akai R, Kohno K (2010) IRE1alpha disruption causes histological abnormality of exocrine tissues, increase of blood glucose level, and decrease of serum immunoglobulin level. PLoS One 5:e13052. doi:10.1371/journal.pone.0013052
40. Iwawaki T, Akai R, Yamanaka S, Kohno K (2009) Function of IRE1 alpha in the placenta is essential for placental development and embryonic viability. Proc Natl Acad Sci USA 106:16657–16662. doi:10.1073/pnas.0903775106
41. Jiang Z, Belforte JE, Lu Y et al (2010) eIF2alpha Phosphorylation-dependent translation in CA1 pyramidal cells impairs hippocampal memory consolidation without affecting general translation. J Neurosci 30:2582–2594. doi:10.1523/JNEUROSCI.3971-09.2010
42. Kakiuchi C, Iwamoto K, Ishiwata M et al (2003) Impaired feedback regulation of XBP1 as a genetic risk factor for bipolar disorder. Nat Genet 35:171–175. doi:10.1038/ng1235
43. Kaushik S, Cuervo AM (2015) Proteostasis and aging. Nat Med 21:1406–1415. doi:10.1038/nm.4001
44. Kennedy BK, Berger SL, Brunet A et al (2014) Geroscience: linking aging to chronic disease. Cell 159:709–713. doi:10.1016/j.cell.2014.10.039
45. Kim B, Kim CY, Lee MJ, Joo YH (2009) Preliminary evidence on the association between XBP1-116C/G polymorphism and response to prophylactic treatment with valproate in bipolar disorders. Psychiatry Res 168:209–212. doi:10.1016/j.psychres.2008.05.010
46. Kondo T, Asai M, Tsukita K et al (2013) Modeling Alzheimer's disease with iPSCs reveals stress phenotypes associated with intracellular abeta and differential drug responsiveness. Cell Stem Cell 4:487–496. doi:10.1016/j.stem.2013.01.009
47. Labbadia J, Morimoto RI (2015) The biology of proteostasis in aging and disease. Annu Rev Biochem 84:435–464. doi:10.1146/annurev-biochem-060614-033955
48. Lee AH, Iwakoshi NN, Glimcher LH (2003) XBP-1 regulates a subset of endoplasmic reticulum resident chaperone genes in the unfolded protein response. Mol Cell Biol 23:7448–7459
49. Lee JH, Won SM, Suh J et al (2010) Induction of the unfolded protein response and cell death pathway in Alzheimer's disease, but not in aged Tg2576 mice. Exp Mol Med 42:386–394
50. Lee JH, Yu WH, Kumar A et al (2010) Lysosomal proteolysis and autophagy require presenilin 1 and are disrupted by Alzheimer-related PS1 mutations. Cell 141:1146–1158. doi:10.1016/j.cell.2010.05.008
51. Lee K, Tirasophon W, Shen X et al (2002) IRE1-mediated unconventional mRNA splicing and S2P-mediated ATF6 cleavage merge to regulate XBP1 in signaling the unfolded protein response. Genes Dev 16:452–466. doi:10.1101/gad.964702
52. Lerner AG, Upton JP, Praveen PV et al (2012) IRE1alpha induces thioredoxin-interacting protein to activate the NLRP3 inflammasome and promote programmed cell death under irremediable ER stress. Cell Metab 16:250–264. doi:10.1016/j.cmet.2012.07.007
53. Loewen CA, Feany MB (2010) The unfolded protein response protects from tau neurotoxicity in vivo. PLoS One 5:e13084. doi:10.1371/journal.pone.0013084
54. Lopez-Otin C, Blasco MA, Partridge L, Serrano M, Kroemer G (2013) The hallmarks of aging. Cell 153:1194–1217. doi:10.1016/j.cell.2013.05.039
55. Lourenco MV, Clarke JR, Frozza RL et al (2013) TNF-alpha mediates PKR-dependent memory impairment and brain IRS-1 inhibition induced by Alzheimer's beta-amyloid oligomers in mice and monkeys. Cell Metab 18:831–843. doi:10.1016/j.cmet.2013.11.002
56. Ma T, Trinh MA, Wexler AJ et al (2013) Suppression of eIF2alpha kinases alleviates Alzheimer's disease-related plasticity and memory deficits. Nat Neurosci 16:1299–1305. doi:10.1038/nn.3486
57. Maly DJ, Papa FR (2014) Druggable sensors of the unfolded protein response. Nat Chem Biol 10:892–901. doi:10.1038/nchembio.1664
58. Martinez G, Vidal RL, Mardones P et al (2016) Regulation of Memory Formation by the Transcription Factor XBP1. Cell Rep 16:1382–1394. doi:10.1016/j.celrep.2016.01.028
59. Maurel M, Chevet E, Tavernier J, Gerlo S (2014) Getting RIDD of RNA: IRE1 in cell fate regulation. Trends Biochem Sci 39:245–254. doi:10.1016/j.tibs.2014.02.008
60. Medinas DB, Hetz C (2013) Proteostasis impairment: at the intersection between Alzheimer's disease and diabetes. Cell Metab 18:771–772. doi:10.1016/j.cmet.2013.11.009
61. Moreno JA, Halliday M, Molloy C et al (2013) Oral treatment targeting the unfolded protein response prevents neurodegeneration and clinical disease in prion-infected mice. Sci Transl Med 5:206ra138. doi:10.1126/scitranslmed.3006767
62. Moreno JA, Radford H, Peretti D et al (2012) Sustained translational repression by eIF2alpha-P mediates prion neurodegeneration. Nature 485:507–511. doi:10.1038/nature11058
63. Nijholt DA, van Haastert ES, Rozemuller AJ, Scheper W, Hoozemans JJ (2012) The unfolded protein response is associated with early tau pathology in the hippocampus of tauopathies. J Pathol 226:693–702. doi:10.1002/path.3969
64. O'Connor T, Sadleir KR, Maus E et al (2008) Phosphorylation of the translation initiation factor eIF2alpha increases BACE1 levels and promotes amyloidogenesis. Neuron 60:988–1009. doi:10.1016/j.neuron.2008.10.047
65. Oakes SA, Papa FR (2015) The role of endoplasmic reticulum stress in human pathology. Annu Rev Pathol 10:173–194. doi:10.1146/annurev-pathol-012513-104649
66. Oakley H, Cole SL, Logan S et al (2006) Intraneuronal beta-amyloid aggregates, neurodegeneration, and neuron loss in transgenic mice with five familial Alzheimer's disease mutations: potential factors in amyloid plaque formation. J Neurosci 26:10129–10140. doi:10.1523/JNEUROSCI.1202-06.2006
67. Ohno M, Chang L, Tseng W et al (2006) Temporal memory deficits in Alzheimer's mouse models: rescue by genetic deletion of BACE1. Eur J Neurosci 23:251–260. doi:10.1111/j.1460-9568.2005.04551.x
68. Ohno M, Cole SL, Yasvoina M et al (2007) BACE1 gene deletion prevents neuron loss and memory deficits in 5XFAD

APP/PS1 transgenic mice. Neurobiol Dis 26:134–145. doi:10.1016/j.nbd.2006.12.008
69. Onate M, Catenaccio A, Martinez G et al (2016) Activation of the unfolded protein response promotes axonal regeneration after peripheral nerve injury. Sci Rep 6:21709. doi:10.1038/srep21709
70. Peng Y, Kim MJ, Hullinger R et al (2016) Improved proteostasis in the secretory pathway rescues Alzheimer's disease in the mouse. Brain 139:937–952. doi:10.1093/brain/awv385
71. Placido AI, Pereira CM, Duarte AI et al (2014) The role of endoplasmic reticulum in amyloid precursor protein processing and trafficking: implications for Alzheimer's disease. Biochim Biophys Acta 1842:1444–1453. doi:10.1016/j.bbadis.2014.05.003
72. Pluquet O, Dejeans N, Bouchecareilh M et al (2013) Posttranscriptional regulation of PER1 underlies the oncogenic function of IREalpha. Cancer Res 73:4732–4743. doi:10.1158/0008-5472.CAN-12-3989
73. Ramirez O, Garcia A, Rojas R, Couve A, Hartel S (2010) Confined displacement algorithm determines true and random colocalization in fluorescence microscopy. J Microsc 239:173–183. doi:10.1111/j.1365-2818.2010.03369.x
74. Reimold AM, Etkin A, Clauss I et al (2000) An essential role in liver development for transcription factor XBP-1. Genes Dev 14:152–157
75. Reinhardt S, Schuck F, Grosgen S et al (2014) Unfolded protein response signaling by transcription factor XBP-1 regulates ADAM10 and is affected in Alzheimer's disease. FASEB J 28:978–997. doi:10.1096/fj.13-234864
76. Sado M, Yamasaki Y, Iwanaga T et al (2009) Protective effect against Parkinson's disease-related insults through the activation of XBP1. Brain Res 1257:16–24. doi:10.1016/j.brainres.2008.11.104
77. Scheper W, Hoozemans JJ (2015) The unfolded protein response in neurodegenerative diseases: a neuropathological perspective. Acta Neuropathol 130:315–331. doi:10.1007/s00401-015-1462-8
78. Selkoe DJ (2008) Soluble oligomers of the amyloid beta-protein impair synaptic plasticity and behavior. Behav Brain Res 192:106–113. doi:10.1016/j.bbr.2008.02.016
79. Shankar GM, Li S, Mehta TH et al (2008) Amyloid-beta protein dimers isolated directly from Alzheimer's brains impair synaptic plasticity and memory. Nat Med 14:837–842. doi:10.1038/nm1782
80. Smith HL, Mallucci GR (2016) The unfolded protein response: mechanisms and therapy of neurodegeneration. Brain 139:2113–2121. doi:10.1093/brain/aww101
81. Song Y, Sretavan D, Salegio EA et al (2015) Regulation of axon regeneration by the RNA repair and splicing pathway. Nat Neurosci 18:817–825. doi:10.1038/nn.4019
82. Stutzbach LD, Xie SX, Naj AC et al (2013) The unfolded protein response is activated in disease-affected brain regions in progressive supranuclear palsy and Alzheimer's disease. Acta Neuropathol Commun 1:31. doi:10.1186/2051-5960-1-31
83. Thal DR, Rub U, Orantes M, Braak H (2002) Phases of A beta-deposition in the human brain and its relevance for the development of AD. Neurology 58:1791–1800
84. Trinh MA, Kaphzan H, Wek RC et al (2012) Brain-specific disruption of the eIF2alpha kinase PERK decreases ATF4 expression and impairs behavioral flexibility. Cell Rep 1:676–688. doi:10.1016/j.celrep.2012.04.010
85. Trinh MA, Ma T, Kaphzan H et al (2014) The eIF2alpha kinase PERK limits the expression of hippocampal metabotropic glutamate receptor-dependent long-term depression. Learn Mem 21:298–304. doi:10.1101/lm.032219.113
86. Uchihara T (2007) Silver diagnosis in neuropathology: principles, practice and revised interpretation. Acta Neuropathol 113:483–499. doi:10.1007/s00401-007-0200-2
87. Unterberger U, Hoftberger R, Gelpi E et al (2006) Endoplasmic reticulum stress features are prominent in Alzheimer disease but not in prion diseases in vivo. J Neuropathol Exp Neurol 65:348–357. doi:10.1097/01.jnen.0000218445.30535.6f
88. Upton JP, Wang L, Han D et al (2012) IRE1alpha cleaves select microRNAs during ER stress to derepress translation of proapoptotic Caspase-2. Science 338:818–822. doi:10.1126/science.1226191
89. Urra H, Dufey E, Lisbona F, Rojas-Rivera D, Hetz C (2013) When ER stress reaches a dead end. Biochim Biophys Acta 1833:3507–3517. doi:10.1016/j.bbamcr.2013.07.024
90. Valdes P, Mercado G, Vidal RL et al (2014) Control of dopaminergic neuron survival by the unfolded protein response transcription factor XBP1. Proc Natl Acad Sci USA 111:6804–6809. doi:10.1073/pnas.1321845111
91. Valenzuela V, Collyer E, Armentano D et al (2012) Activation of the unfolded protein response enhances motor recovery after spinal cord injury. Cell Death Dis 3:e272. doi:10.1038/cddis.2012.8
92. Verwey NA, Hoozemans JJ, Korth C et al (2013) Immunohistochemical characterization of novel monoclonal antibodies against the N-terminus of amyloid beta-peptide. Amyloid 20:179–187. doi:10.3109/13506129.2013.797389
93. Viana RJ, Nunes AF, Rodrigues CM (2012) Endoplasmic reticulum enrollment in Alzheimer's Disease. Mol Neurobiol 46:522–534. doi:10.1007/s12035-012-8301-x
94. Vidal RL, Figueroa A, Court FA et al (2012) Targeting the UPR transcription factor XBP1 protects against Huntington's disease through the regulation of FoxO1 and autophagy. Hum Mol Genet 21:2245–2262. doi:10.1093/hmg/dds040
95. Vorhees CV, Williams MT (2006) Morris water maze: procedures for assessing spatial and related forms of learning and memory. Nat Protoc 1:848–858. doi:10.1038/nprot.2006.116
96. Walter P, Ron D (2011) The unfolded protein response: from stress pathway to homeostatic regulation. Science 334:1081–1086. doi:10.1126/science.1209038
97. Wang M, Kaufman RJ (2016) Protein misfolding in the endoplasmic reticulum as a conduit to human disease. Nature 529:326–335. doi:10.1038/nature17041
98. Xu T, Yang L, Yan C et al (2014) The IRE1alpha-XBP1 pathway regulates metabolic stress-induced compensatory proliferation of pancreatic beta-cells. Cell Res 24:1137–1140. doi:10.1038/cr.2014.55
99. Yang DS, Stavrides P, Mohan PS et al (2011) Reversal of autophagy dysfunction in the TgCRND8 mouse model of Alzheimer's disease ameliorates amyloid pathologies and memory deficits. Brain 134:258–277. doi:10.1093/brain/awq341
100. Yang DS, Stavrides P, Saito M et al (2014) Defective macroautophagic turnover of brain lipids in the TgCRND8 Alzheimer mouse model: prevention by correcting lysosomal proteolytic deficits. Brain 137:3300–3318. doi:10.1093/brain/awu278
101. Yang J, Cheng D, Zhou S et al (2015) Overexpression of X-Box binding protein 1 (XBP1) correlates to poor prognosis and Up-regulation of PI3 K/mTOR in human osteosarcoma. Int J Mol Sci 16:28635–28646. doi:10.3390/ijms161226123
102. Yang W, Zhou X, Zimmermann HR et al (2016) Repression of the eIF2alpha kinase PERK alleviates mGluR-LTD impairments in a mouse model of Alzheimer's disease. Neurobiol Aging 41:19–24. doi:10.1016/j.neurobiolaging.2016.02.005
103. Yoshida H, Matsui T, Yamamoto A, Okada T, Mori K (2001) XBP1 mRNA is induced by ATF6 and spliced by IRE1 in response to ER stress to produce a highly active transcription factor. Cell 107:881–891